Solvation of excess electrons in supercritical ammonia

Javier Rodriguez, Munir S. Skaf, and Daniel Laria

Citation: The Journal of Chemical Physics **119**, 6044 (2003); doi: 10.1063/1.1601215
View online: http://dx.doi.org/10.1063/1.1601215
View Table of Contents: http://scitation.aip.org/content/aip/journal/jcp/119/12?ver=pdfcov
Published by the AIP Publishing

Solvation of excess electrons in supercritical ammonia

Javier Rodriguez
Unidad Actividad Química, Comisión Nacional de Energía Atómica, Avenida Libertador 8250, 1429, Buenos Aires, Argentina, and Escuela de Ciencia y Tecnología, Universidad Nacional de General San Martín, Calle 91 3391, 1652, San Martín, Pcia. de Buenos Aires, Argentina

Munir S. Skaf
Instituto de Química, Universidade Estadual de Campinas, Cx. P. 6154, Campinas, SP 13083-970, Brazil

Daniel Laria
Unidad Actividad Química, Comisión Nacional de Energía Atómica, Avenida Libertador 8250, 1429, Buenos Aires, Argentina, and Departamento de Química Inorgánica, Analítica y Química-Física e INQUIMAE, Facultad de Ciencias Exactas y Naturales, Universidad de Buenos Aires Ciudad Universitaria, Pabellón II, 1428, Buenos Aires, Argentina

(Received 27 February 2003; accepted 24 June 2003)

Molecular dynamics simulations have been performed to study equilibrium and dynamical aspects of solvation of excess electrons in supercritical ammonia along the $T=450$ K isotherm. The interval of supercritical densities investigated spans from typically dense liquid down to dilute vapor ambients. Equilibrium aspects of solvation were analyzed using combined path integral-molecular dynamics techniques. The transition from localized to quasifree states, described in terms of the isomorphic electron-polymer spatial extent, was observed at approximately one fourth of the triple point density, a value somewhat higher than that recently reported for supercritical water [D. Laria and M. Skaf, J. Phys. Chem. A **106**, 8066 (2002)]. The density of electronic eigenstates shows typically one *s*- and three *p*-like bound states that gradually lose their symmetry characteristics as the density lowers. The computed ground state absorption spectrum exhibits redshifts in the absorption bands as the density decreases; these shifts are much larger than those reported by pulse radiolysis experiments. By performing adiabatic dynamics, we also investigate mechanisms for solvent relaxation at high and intermediate supercritical densities following a vertical excitation of the electron. © *2003 American Institute of Physics.* [DOI: 10.1063/1.1601215]

I. INTRODUCTION

Chemical reactivity in supercritical polar environments represents the subject of a wealth of ongoing research work due to its important technological applications.[1–3] The main reasons for this interest reside in the profound changes that take place in many physicochemical properties of these systems, compared to what is normally perceived at more conventional conditions. At supercritical temperatures, large displacements in chemical equilibria[4] and solvation-induced modifications in the reaction rates by several orders of magnitude[5] are not uncommon, a fact that reveals the importance of the reactant complex-solvent coupling as a key factor determining the channels that drive the dynamics of the reactive processes.

Microscopic aspects of polar solvation may be examined by a wide variety of molecular solutes. Excess electrons provide an excellent example of very sensible probes to gain direct experimental information about the changes that operate in the structure of a solvent to host a negatively charged solute. Given the inherently quantum nature of the electron, its solvation normally exhibit well differentiated characteristics from what is usually encountered in cases of simpler, classical, anionic solutes. Most notably, is the existence of the electronic localization phenomenon, reflected in the dramatic drop that appears in the electronic drift mobility.[6,7] From a microscopic point of view, the transition from delocalized to localized states is usually described in terms of the spatial confinement of the electronic density within a solvent cavity, whose average shape fluctuations can normally be inferred from the analysis of the position and line shape of the electron absorption band.[8–10] Moreover, time resolved spectroscopy experiments[11–13] open new venues for acquiring detailed information on the relevant time scales involved in the solvation dynamics as well.

The subject of the present paper deals with equilibrium and dynamical aspects of the electronic states in supercritical ammonia (SCA). In a much broader context, the analysis of electronic states in supercritical environments—including polar and nonpolar ambients, such as the case of noble gases[14]—is particularly appropriate to investigate density effects on the electronic localization, since it allows sweeping the whole fluid density range without worrying about the occurrence of liquid–gas phase transitions in the host fluid. In the specific case of electron solvation in SCA, the subject has received considerable attention in recent times. Experimental results for the electron mobility in SCA at temperatures fifty degrees above the critical one ($T_c^a=405$ K) suggest a transition from delocalized to localized states in the density range of approximately 0.02 times the normal liquid density. Interestingly, in this thermal regime the drift mobil-

ity also exhibits a nonmonotonic density dependence, with a minimum located slightly below the critical density.[7,15,16] These changes contrast sharply with the apparently much weaker sensitivity of the position of the main absorption peak in a wide density interval of supercritical states.[8,9] From the theoretical point of view, computer simulations have been conducted to analyze details of the electronic states in bulk ambients[17–20] at lower temperatures and nanoclusters[21,22] as well. In this work, we extend these previous studies to higher temperatures and lower solvent densities, applying combined path integral-molecular dynamics (PIMD) simulation techniques. We are interested not only in equilibrium characteristics of the excess electron solvation but we also make a first exploratory analysis of the early stages of the solvation dynamics that follows a vertical photoexcitation of the solute using the adiabatic approximation for the quantum electronic dynamics.

In a related context, we recently examined electronic solvation in supercritical water (SCW).[23] Our simulation experiments found that at temperatures slightly above the critical one ($T_c^w = 647\,\mathrm{K}$), the localization transition in water, expressed in terms of the spatial extent of the electron, takes place in a density range roughly between one and two tenths of the triple point density. This value is substantially higher than that previously estimated from mobility measurements at nearly critical conditions.[6] Moreover, we also found that, similarly to what is found at lower temperatures,[19] the broad absorption spectrum at supercritical conditions comprises transitions from an *s*-ground state into three *p*-like excited states, exhibiting a considerable redshift as we move to lower densities, somewhat larger than that found in experiments.[24]

Yet, for the particular case of the electronic solvation in ammonia, we anticipate several differences from what we have already observed in supercritical aqueous scenarios: First, compared to what is found in water, changes in temperature and density seem to promote less dramatic disruptions in the intermolecular spatial correlations of ammonia. Neutron diffraction[25] and computer simulation experiments[26] performed for supercritical ammonia show only a weak loss of structure in the site–site correlation functions, especially those pertaining to N–H pairs. Secondly, the differences in the critical temperatures of both fluids should lead to more important quantum thermal effects on the electron solvation for the case of ammonia. In view of the fact that the solvation of excess electrons results from a complex interplay between a variety of phenomena, including: (i) packing effects and specific intermolecular connectivity of the host fluid, (ii) thermal quantum fluctuations, and (iii) the specific characteristics of the coupling between the electron and the solvent response, the simulation analysis presented here is expected to provide further insights into the microscopic nature of these systems.

The organization of this work is as follows: In Sec. II, we present details of the model and the simulation methodology. Equilibrium results from the PIMD runs and dynamical information about the response of a selected supercritical states are presented in Sec. III. The main conclusion are left for Sec. IV.

II. METHODS AND MODEL

A. Path integral MD

The systems under investigation consists of a quantum electron coupled to a classical bath containing $N_a = 216$ ammonia molecules. Equilibrium properties of the excess electron solvation have been investigated using Feynman's path integral formulation of quantum statistical mechanics.[27] Within this formalism, the canonical partition function of the system, Q, is written as

$$Q \propto \int \mathrm{d}\{\mathbf{R}\} \exp(-\beta V_{\mathrm{cl}}[\{\mathbf{R}\}]) \int \cdots \int \mathcal{D}[\mathbf{r}(t)] \times \exp(-S[\mathbf{r}(t),\{\mathbf{R}\}]), \tag{1}$$

where $V_{\mathrm{cl}}[\{\mathbf{R}\}]$ denotes the potential energy for the classical particles with coordinates $\{\mathbf{R}\}$; $\mathbf{r}(t)$ is the electron position at the imaginary time t; and $\mathcal{D}[\mathbf{r}(t)]$ represents the path integral. The action functional $S[\mathbf{r}(t),\{\mathbf{R}\}]$ is given by

$$S[\mathbf{r}(t),\{\mathbf{R}\}] = \frac{1}{\beta\hbar} \int_0^{\beta\hbar} \mathrm{d}t \left[\frac{1}{2} m_e \dot{\mathbf{r}}^2(t) + V_{es}[\mathbf{r}(t),\{\mathbf{R}\}] \right], \tag{2}$$

where m_e is the electron mass and $V_{es}[\mathbf{r}(t),\{\mathbf{R}\}]$ represents the coupling between the electron and solvent molecules. The rest of the symbols retain their usual meaning. Intermolecular interactions between ammonia particles included in V_{cl} were described using the four site model of Impey *et al.*[28] For the electron–solvent interactions, V_{es}, we adopted the pseudopotential proposed by Sprik *et al.*[17] In its simplest form, this local pseudopotential incorporates only bare Coulomb contributions between the electron and the solvent sites, while short range repulsions due to exchange forces and polarizability terms are both neglected. Although more elaborate model potentials exist in the literature,[29,30] at this stage we did not investigate further possible effects from repulsions and/or polarizability contributions. The incorporation of the former is surely not crucial to provide a reasonable description even in high density polar environments, where the sole incorporation of Coulomb forces seems adequate to describe the main features of solvated electrons.[17–20] On the other hand, contributions from polarizability effects in highly packed liquid ammonia seem to be of some relevance but not a key ingredient,[30] although we do not discard that the situation may change considerably in density regimes where the distance between neighboring solvent molecules is larger than the thermal wavelength of the electron.

At present, there exist well tested algorithms to sample thermal fluctuations of the electron path according to the action given in Eq. (2) in an efficient way. The methodologies rely on the isomorphism[31] established between the statistical mechanics of the quantum electron path and that of a classical cyclic polymer containing P pseudoparticles (''beads'') with coordinates $\mathbf{r}_i$. For a finite value of P, the quantum partition function in Eq. (1) reduces to that of a classical system interacting with an effective potential given by

$$V_{\text{eff}} = V_{\text{cl}} + \frac{P m_e}{2(\beta\hbar)^2} \sum_{i=1}^{P} (\mathbf{r}_i - \mathbf{r}_{i+1})^2 + \frac{1}{P} \sum_{i=1}^{P} V_{es}[\{\mathbf{r}_i\}, \{\mathbf{R}\}]. \tag{3}$$

To sample configuration space we implemented a combined path integral-molecular dynamics (PIMD) algorithm that includes a reversible, multiple time scale integrator of Newton's equations of motion and the staging ansatz.[32]

To simulate canonical dynamics, chains of three Nosé–Hoover thermostats set at $T = 450\,\text{K}$ were coupled to each Cartesian coordinate of the electron polymer. The classical bath was also coupled to an identical thermostat chain. This thermal regime—which is roughly 10% above the experimental critical temperature of ammonia—was deliberately chosen so as to establish a correspondence with our recent PIMD study of supercritical water performed at a similar reduced temperature.[23] Similarly, we investigated the supercritical density interval $0.033\,\text{g cm}^{-3} \leqslant \rho_a \leqslant 0.72\,\text{g cm}^{-3}$, $(\rho_c^a = 0.236\,\text{g cm}^{-3})$, which spans from highly packed down to low density gaseous ambients. A few test runs were also performed at low temperature, at the experimental ammonia triple point: $\rho_t^a = 0.723\,\text{g cm}^{-3}$, $T_t^a = 260.5\,\text{K}$. Two different time steps were used: $\Delta t = 10^{-2}$ fs to integrate the classical bath variables and $\delta t = \Delta t/3$ to evolve the rest of the fast dynamical variables (including the thermostats). The number of beads and staging masses were set to $P = 1000$ and $j - 1 = 49$, respectively. The masses of the electron pseudoparticles were taken to be equal to the electron mass, while the rest of the classical particles were assigned masses equal to 10^{-2} times their actual values. The masses of the thermostat chains attached to the electronic degrees of freedom were set equal to $Q_e^{\text{stage}} = \beta\hbar^2/P$ and $Q_e^{\text{end}} = jQ_e^{\text{stage}}$ for the stage and end beads, respectively. The masses of the chain of thermostats coupled to the classical particles were taken as $Q_1 = N_{\text{cl}}/(\beta\omega_{\text{LJ}})$ and $Q_i = Q_1/N_{\text{cl}}\,(i = 2,3)$, where N_{cl} is the number of classical degrees of freedom in the system and ω_{LJ} is the frequency at the minimum of the nitrogen–nitrogen Lennard-Jones interaction in ammonia. Constraints imposed on the intramolecular distances and on the particle positions were handled with the SHAKE algorithm.[33] All simulations included an equilibration period of approximately $10^5\Delta t$, followed by trajectories of typical length $5-10\times10^5\Delta t$ used to evaluate the statistical properties of the system.

B. Adiabatic dynamics

Dynamical information about the electronic states was extracted from a second set of simulations, performed using a quantum adiabatic dynamics scheme. The electronic wave functions was expressed in terms of 16^3 plane waves, uniformly distributed over the spatial extent of the simulation box. For a given configuration of the classical bath, electron eigenvalues $\{\epsilon_n\}$ and eigenfunctions $\{\psi_n\}$ were computed by means of the block Lanczos procedure combined with the split operator fast Fourier transform techniques described in Ref. 34. Quantum forces acting of the classical particles were computed using the Hellmann–Feynman expression,

$$\mathbf{F}_i^q = -\nabla_{\mathbf{R}_i}\epsilon_n(\{\mathbf{R}\}). \tag{4}$$

In this equation, $\mathbf{F}_i^q$ represents the contribution to the force acting on the ith particle due to the presence of the quantum electron. We explicitly indicated that the eigenstates (labeled n) are dependent on the specific solvent configuration considered. The time step for these simulation runs was set to 0.1 fs.

In all cases, Lennard-Jones interactions were cut at half the simulation box length, while long ranged interactions derived from the different Coulomb terms were handled by Ewald sum techniques,[35,36] assuming the presence of a uniform neutralizing background.

Information about dynamical responses of spectroscopic relevance, can be conveniently extracted by performing nonequilibrium, relaxation runs. In the present case, these simulation experiments basically consisted in performing an initial equilibrium trajectory, in which the quantum forces on the classical particles were taken with the electron occupying the instantaneous ground state $\epsilon_0(\{\mathbf{R}_N\})$. From this trajectory, solvent configurations separated by 2 ps intervals were adopted as initial conditions for relaxation trajectories, during which quantum forces were taken according to Eq. (4), with the system propagated in the presence of the electron in its (instantaneous) first excited state. These trajectories were used to compute nonequilibrium response functions $S_{\mathcal{O}}(t)$ for different relevant observables $\mathcal{O}(t)$, namely,

$$S_{\mathcal{O}}(t) = \langle \mathcal{O}(t) \rangle_{\text{ne}}, \tag{5}$$

where $\langle \cdots \rangle_{\text{ne}}$ denotes an average sampled from the distribution of nonequilibrium initial conditions and the time origin was set to coincide with the electronic excitation.

III. RESULTS

A. Equilibrium solvation

The extent of the electron localization in the different supercritical environments can be conveniently probed by analyzing the behavior of the correlation length of the electron polymer $\mathcal{R} = \mathcal{R}(\beta\hbar/2)$, where $\mathcal{R}^2(t)$ is defined by

$$\mathcal{R}^2(t - t') = \langle |\mathbf{r}(t) - \mathbf{r}(t')|^2 \rangle; \quad 0 \leqslant t - t' \leqslant \beta\hbar. \tag{6}$$

Solvated electrons in water and ammonia in the vicinity of their corresponding triple points are known to be localized and characterized by length scales $\mathcal{R}$ of similar order of the size of a solvent molecule, i.e., intermediate between 3 and 4 Å.[17,37] On the other hand, and for the particular case of low density, steamlike, aqueous supercritical ambients, say $\rho_w < 0.1\,\text{g cm}^{-3}$, the correlation function $\mathcal{R}(t)$ looks similar to that corresponding to a Gaussian, noninteracting polymer, with the longest correlation length comparable to λ_{DB}, the electron de Broglie thermal wavelength.[23]

In Fig. 1 we present results for $\mathcal{R}$ in SCA, at $T^* = 1.10$. We have also included results for SCW along the same (reduced temperature) isotherm. In order to facilitate the comparison between results from the two fluids, it is convenient to scale all temperatures and densities by the corresponding critical $(T^* = T/T_c)$ and triple point $(\rho^* = \rho/\rho_t)$ values, respectively. The sharp drop to practically half of its ideal, i.e., noninteracting, $\rho = 0$, value within a narrow density interval along with a change in the slope of the curve,

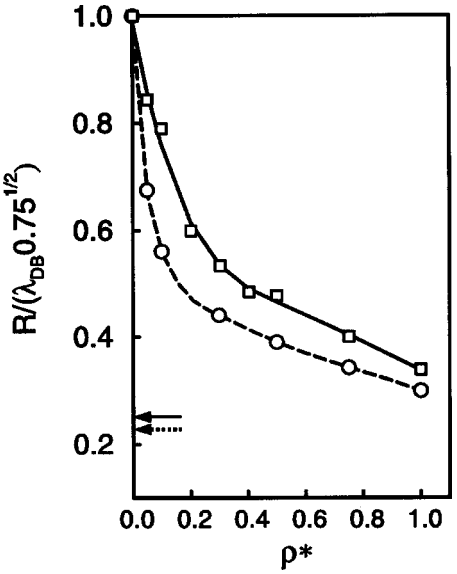

FIG. 1. Correlation length for the electron-polymer along the $T^*=1.10$ isotherm for supercritical ammonia (solid line, squares) and supercritical water (dashed line, circles). The arrows indicate the correlation lengths for solvated electrons at the corresponding triple points of the two fluids.

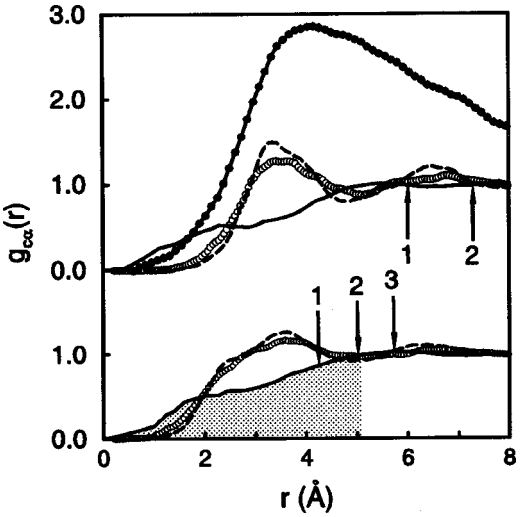

FIG. 2. Centroid–solvent pair correlation functions for different SCA states at $T^*=1.10$. Top curves: $g_{cN}(r)$; bottom curves: $g_{cH}(r)$. $\rho^*=0.05$: solid lines; $\rho^*=1$: open circles. Also shown are the profiles for electron–solvent correlation at the triple point (dashed lines), and for SCW ($\rho^*=0.1$ and $T^*=1.10$; black circles). The arrows indicate the coordination numbers at selected distances and the shaded area represents the electron spatial extent expressed in terms $\mathcal{R}/2$, at the lowest density.

reveal that the onset of the electronic localization in SCA, as reflected by the polymer size, takes place at $\rho_a^*\approx 0.25$. Comparison with the curve for SCW, where the transition takes place at $\rho_w^*\approx 0.15$, shows that polarization fluctuations in the latter fluid are more ''effective'' in promoting electronic localization. This feature can be simply understood in view of the stronger polar character of bulk water compared to ammonia,[38] and the larger length scales describing the quantum thermal fluctuations of the electron: $\lambda_{DB}(T=450\,\mathrm{K})\simeq 18\,\text{Å}$ and $\lambda_{DB}(T=650\,\mathrm{K})\simeq 14\,\text{Å}$. Consequently, both effects should lead to weaker electron–solvent Coulomb coupling. As a result, the actual size of the electron–polymer in SCA is, in all cases, much larger than in SCW. A similar observation holds when comparing results of electronic sizes in the two fluids at their corresponding triple points, indicated by the arrows in Fig. 1.

The analysis of electron centroid–solvent spatial correlation provides complementary information about the characteristics of the electronic delocalization. The electron centroid is defined as $\mathbf{r}_c=(1/\beta\hbar)\int_0^{\beta\hbar}\mathbf{r}(t)dt$. In Fig. 2 we present results for different solvent–centroid pair correlation function $g_{c\alpha}(r)$, (α=N,H),

$$g_{c\alpha}(r)=\frac{1}{4\pi r^2\rho_\alpha}\left\langle\sum_{i=1}^{N_a}\delta(|\mathbf{r}_c-\mathbf{R}_i^\alpha|-r)\right\rangle, \tag{7}$$

where $\mathbf{R}_i^\alpha$ denotes the coordinate of site α in the ith ammonia molecule and ρ_α the corresponding site density. Compared to the spatial correlations at the triple point (dashed lines), the profiles for high density, supercritical states (empty symbols) show a moderate loss of structure in the close vicinity of the electron centroid, where a first solvation shell is still perceptible. A reduction in density leads to more dramatic changes since, for example, at $\rho_\alpha^*=0.05$, one obtains featureless profiles (solid lines) that monotonously approach their limiting, $g_{c\alpha}=1$, value within a distance interval of $\approx$5–6 Å away from the electron centroid. The ammonia profiles should be contrasted to those for SCW at the same reduced density—upper set of curves in Fig. 2 (filled symbols)—where the effective electron–solvent coupling is still strong enough to promote a considerable enhancement of the local solvent density fields around the quantum solute. For ammonia, in

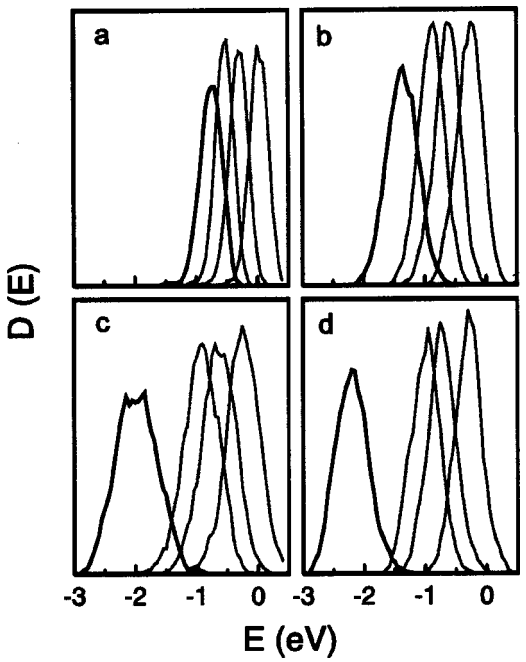

FIG. 3. Density of bound electronic states for different densities along the $T^*=1.1$ isotherm. (a) $\rho_a^*=0.35$; (b) $\rho_a^*=0.5$; (c) $\rho_a^*=1.0$. Also shown are the results for the triple point (d). Solid lines correspond to the ground states. Thin lines correspond to the first, second, and third quasidegenerate excited states.

contrast, the electron appears too diffuse ($\mathcal{R}\approx 10$ Å) and is not able to promote any relevant ''clustering'' of solvent particles in its immediate vicinity.

The analysis of the coordination numbers expressed in terms of the running integrals of the different $g_{c\alpha}(r)$, provides an idea of the extent of electron tunneling into spatial domains of the solvent. The coordination numbers at different distances from the electron centroid are indicated by arrows in Fig. 2. At the lowest density considered, there is typically two hydrogen atoms within a distance r from the electron centroid comparable to the gyration radius of the polymer, approximated by $\approx\mathcal{R}/2$ (see Fig. 2).

B. Density of states and absorption spectra

Figure 3 shows results for $D(E)$, the electron density of states defined as

$$D(E)=\left\langle \sum_{\epsilon_i<0} \delta(\epsilon_i-E)\right\rangle. \tag{8}$$

The profiles were constructed by diagonalizing the electronic Schrödinger equation for 200 statistically independent solvent configurations, obtained along the PIMD run. Results are shown for the ground state (solid lines) and the three lowest lying excited states (dashed lines). The corresponding density of states for $\rho_a^*=0.35$, 0.5, and 1 along with results at the triple point are depicted in panels (a)–(d). The profiles reveal that the main effects of lowering the solvent density are reflected in a gradual shift in the position of the ground state distribution towards higher energies, while the distributions for the three excited states remain practically unchanged. A comparison between panels (c) and (d) shows that, as T^* goes from 1.10 to 1.0, there is only a slight broadening in the distribution of ground state energies due to larger shape fluctuations in the electron trapping cavities. This indicates that temperature effects are much less important than density effects upon $D(E)$. The physical picture that emerges from these observations suggests a reduction in the energy gaps due to the larger box length at lower densities, which seems consistent with a simple picture of a quantum particle in a fluctuating soft box model.

Similarly to what has been found at subcritical conditions using a set of mobile Gaussian basis,[19] the low lying bound states at supercritical conditions correspond to a ground *s*-like state and three, quasidegenerate, somewhat more delocalized excited states, with *p*-like characteristics. A more vivid picture of the overall shape of the electronic densities can be acquired from Fig. 4, where we present a series of two-dimensional projections $\tilde{\rho}_l\,(l=0,1)$,

$$\tilde{\rho}_l(x_j,x_k)=\int |\psi_l|^2 \mathrm{d}x_i\,, \tag{9}$$

where (x_i,x_j,x_k) are the three principal axis of the simulation box. At a first glance, the gross features of the symmetry characteristics of the ground and first excited states in high density environments are self-evident: Most noteworthy, is a nearly Gaussian-type profile for the ground electronic state, and the clear presence of a nodal plane in the first excited state. However, as we move to lower densities, the shape of the electron wave functions become more distorted preventing a clear characterization in terms of their symmetry properties.

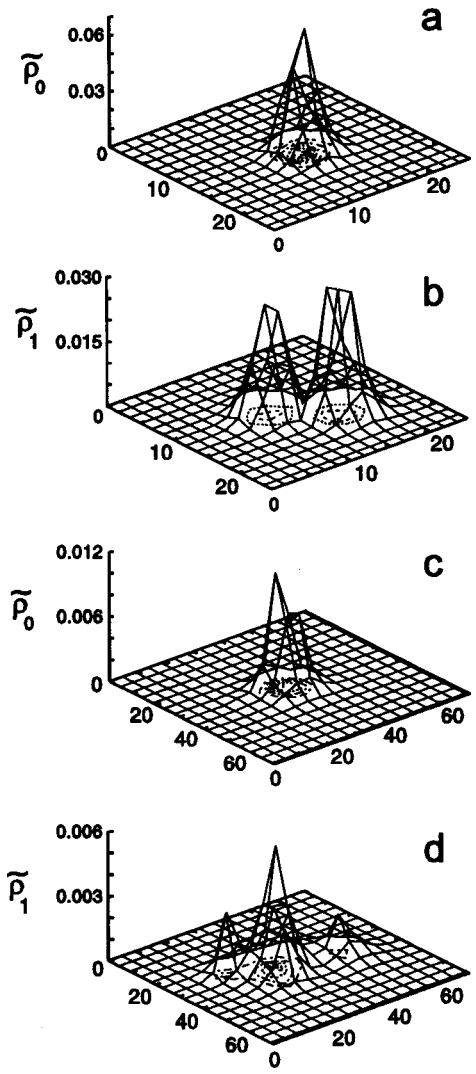

FIG. 4. Two-dimensional projections $\tilde{\rho}_i$ (in Å^{-2}) of the ground and first excited electronic state for solvated electrons in SCA. Panels (a) and (b) correspond to $\rho_a^*=1$; panels (c) and (d) correspond to $\rho_a^*=0.05$. Box lengths are expressed in Å.

The ground state absorption spectra, $I(\omega)$, at four supercritical densities computed within the Franck–Condon approximation, namely,

$$I(E)\propto E(1-e^{-\beta E})\left\langle \sum_{i>0,\epsilon_i<0} |\langle\psi_0|\hat{\boldsymbol{\mu}}|\psi_i\rangle|^2\,\delta(\epsilon_i-\epsilon_0-E)\right\rangle, \tag{10}$$

are presented in Fig. 5, where we have also included results for the triple point. Compared to the experimental data,[8] the position of the maximum at the latter conditions is slightly blue shifted ($\sim$0.2 eV), as has been noted elsewhere.[19] Anyhow, the overall simulated line shape is rather asymmetric in accordance with the experimental result, although its high energy branch is somewhat less developed. Consistently with the behavior exhibited by the density of states (Fig. 3), temperature alone does not lead to significant changes in the absorption band. Similar features have also been found in

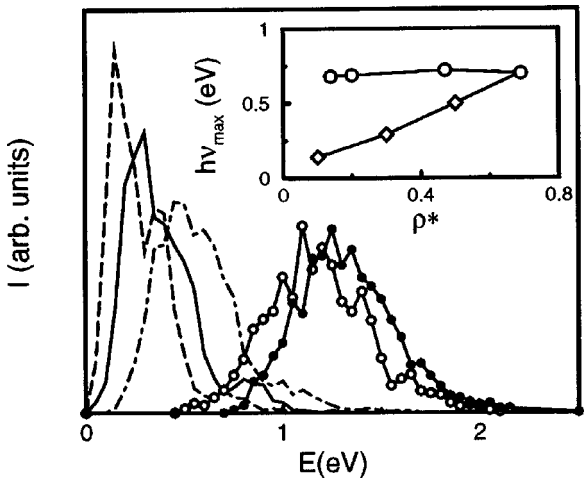

FIG. 5. Electron absorption spectra for different densities at $T^*=1.1$ isotherm. $\rho_a^*=0.075$ (dashed lines); $\rho_a^*=0.35$ (solid lines); $\rho_a^*=0.5$ (dotted–dashed lines); $\rho_a^*=1$ (open circles). Also shown results for the triple point (black circles). The inset shows the density dependence of the absorption maxima in the low density interval investigated. Diamonds: this work; circles: Refs. 9 and 10.

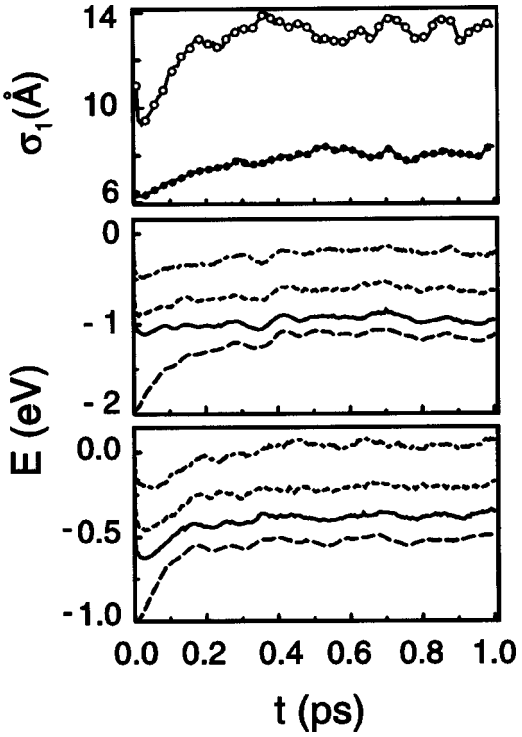

FIG. 6. Top panel: Relaxations for the electron size; $\rho_a^*=1$ (black circles); $\rho_a^*=0.3$ (open circles). Middle ($\rho_a^*=1$) and bottom ($\rho_a^*=0.3$) panels: dynamical history of the adiabatic electronic eigenstates. The results correspond to supercritical states and the electron was promoted from the equilibrium ground state to the first excited state at $t=0$.

simulations of hot and supercritical water, including computations performed with a polarizable electron–solvent pseudopotential.[39] At lower densities ($\rho_a^*\leqslant 0.5$), however, the maxima of our simulated spectra present redshifts much larger than those experimentally reported at similar thermodynamic conditions,[9,10] where very broad absorption bands for solvated electrons in the 0.1–0.2 eV region are reported for $0.15\leqslant\rho_a^*\leqslant 0.7$ along the $T^*=1.05$ isotherm. In principle, the insensitivity of the position of absorption maxima in a broad density interval found in the experiments could be interpreted as the absence of any relevant modifications of the solvent density fields in the close vicinity of the solute. In other words, at low densities, the electron–solvent coupling would induce a considerable ''clustering'' of the solvent around the electron, that would experience practically no modifications as the density lowers. As we mentioned in previous paragraphs, this interpretation clashes with the results of our simulations, which do not show evidences of any relevant solvent clustering around the electron. At this point, one could envisage several possible reasons for the lack of accordance. Perhaps the first one to be considered is the crude description of the electron–solvent pseudopotential and most notably, the absence of polarizability contributions that would eventually promote a stronger solvent–electron coupling in the low density regime. Anyhow, we anticipate that the presence of ''clustering'' or the explicit inclusion of polarization fluctuations in the electron–solvent coupling are likely to be insufficient to explain the weak dependence of position of the maximum of the absorption spectrum; results for SCW using a much more elaborate electron–solvent pseudopotential do show considerable ''clustering'' and yet, similar redshifts to those presented here still persist in the low density region. As such, the limitations of our model Hamiltonian remains an open question that certainly deserves deeper investigations.

C. Solvation dynamics upon electronic excitation

Our dynamical description of the solvation will be restricted to the relaxation process that follows a vertical excitation of the excess electron, within the adiabatic quantum dynamics approximation. To gain a preliminary insight on the problem, it will be instructive to briefly address the characteristics of the time evolution of a couple of relevant observables. Figure 6 contains dynamical information about the electron size and the four lowest lying adiabatic states at two SCA densities, following the promotion of the electron at $t=0$ from the equilibrium ground state to the first excited state. The electron size was estimated as

$$\sigma_1^2=\langle\psi_1|(\mathbf{r}-\overline{\mathbf{r}}_1)^2|\psi_1\rangle, \tag{11}$$

with $\overline{\mathbf{r}}_1=\langle\psi_1|\mathbf{r}|\psi_1\rangle$. In the top panel, we observe that during the first 20–30 fs from the excitation, the spatial extent of electronic density presents a sudden drop—barely perceptible in the high density case—before reversing its initial trend towards more extended states. After ≈200–300 fs, the electronic wave functions at both densities have already leveled off to their asymptotic values, resulting in final spreads intermediate between 20% and 40% larger that the corresponding initial values. The resulting degree of electronic delocalization upon excitation is rather large, and, in both cases, exceeds largely the average distance between solvent particles $\sim\rho_a^{-1/3}$. A similar nonmonotonic behavior was also detected in the time evolution of the instantaneous eigenstates (middle and bottom panels of Fig. 6), with the exception of the ground state (long-dashed curves), which shift to

higher values of energy more abruptly,[40,41] reducing the energy gap with the occupied first excited states to nearly 0.25 and 0.15 eV, for high and low density supercritical states, respectively. These observations are consistent with the physical picture according to which the dynamics of the solvent during the earliest stages of the solvation are governed by the momenta prevailing before the excitation of the probe, thus exhibiting ''ballistic'' or inertial characteristics. This leads to the sudden moderate contraction of the electronic density, followed by a subsequent gradual charge delocalization that takes place within a time interval of 200–330 fs. The latter change results from the weakening of the effective solvent–electron coupling as the solvent modifies its original solvation structure to accommodate now a much more diffuse ''anion.'' Incidentally, within this interpretation, one can also argue that such a less favorable electron solvation should be counterbalanced by a stabilization of the solvent–solvent interactions. Unfortunately, given the disparity between the magnitudes of the electron–solvent and solvent–solvent energy contributions, our simulation experiments were not sufficiently accurate to confirm this assertion.

The fact that the energy gap between the ground and the first excited electronic states reduces considerably upon excitation—becoming, in fact, comparable to the nuclear thermal energy fluctuations—reveals that the excited state dynamics is expected to be influenced by nonadiabatic effects. Moreover, previous studies of solvation dynamics of excess electrons in water at room temperature did show that the nonadiabatic decay rate is inversely proportional to the magnitude of the energy gap and that the average lifetime of the excited electronic state before decaying to the ground state in aqueous ambients is intermediate between 500 fs and 1 ps.[40,41] Consequently, since these time scales are similar to those observed for the relaxation of the adiabatic states shown in Fig. 6, the validity of our adiabatic dynamical description for periods beyond these values will only be marginally satisfied. Moreover, the fact that the solvent response decays a sizable portion within the first few hundreds of femtoseconds suggests that a more detailed analysis of the solvation dynamics should be performed including the possibility of coupling with the intramolecular motions. Although this is certainly a reasonable assumption, specially in view of the magnitude of the totally symmetric bending frequency of ammonia ($\nu_b = 932\ \mathrm{cm}^{-1}$),[42] previous results on the electronic solvation response of water at ambient conditions show that the relaxation chanels involving intramolecular modes of the solvent contribute mildly to the response.[36,40,43,44]

Bearing these caveats in mind, we now turn the analysis of the relaxation of the observable of spectroscopic relevance, namely, the normalized nonequilibrium response function for the solvent energy gap, $S_E(t)$, defined as

$$S_E(t) = \frac{\langle \Delta E(t) - \Delta E(\infty) \rangle_{\mathrm{ne}}}{\langle \Delta E(0) - \Delta E(\infty) \rangle_{\mathrm{ne}}}, \tag{12}$$

where $\Delta E = \epsilon_1(t) - \epsilon_0(t)$ represents the instantaneous electronic energy gap. In Fig. 7 we depict results for $S_E(t)$ at the supercritical densities corresponding to those shown in Fig. 6. The high density curve exhibits a clear bimodal character:

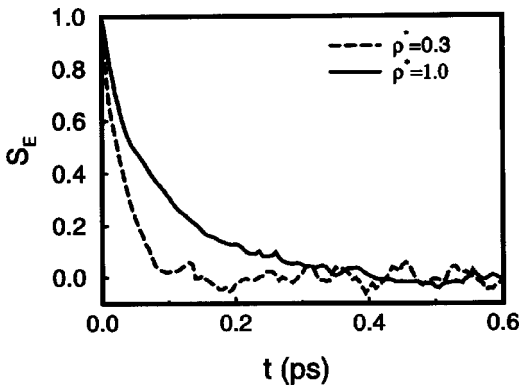

FIG. 7. Normalized nonequilibrium response function for the solvent energy gap at two different supercritical densities of ammonia.

a Gaussian-type initial decay accounting for a sizable fraction (~40%–50%) of the total decay, followed by a much slower, diffusive tail that accounts for the manifold of slow processes, mainly rotational and spatial diffusive motions, that drive the long time response of the solvent. Notice, however, that this bimodal character is much less prominent at lower densities, and that the response practically vanishes after a sharp decay lasting ~100 fs. In order to obtain estimates for the time scales involved in the initial relaxation, we have fitted the $t < 100$ fs portions of the simulated $S_E(t)$ by a simple Gaussian: $S_E(t) \approx \exp[-\frac{1}{2}(\omega_s t)^2]$; ω_s represents the solvation frequency, normally an equilibrium quantity that determines the width or the initial curvature of the response. The short time behavior of both curves shown in Fig. 7 can be equally well reproduced by assuming $\omega_s \simeq 27-30\ \mathrm{fs}^{-1}$. Interestingly, this characteristic solvation frequency appears to be related to the average squared free rotation frequency,[45]

$$\omega_s^2 \approx \alpha_s \omega_f^2, \tag{13}$$

where

$$\omega_f^2 = \frac{2k_B T}{I_{\mathrm{eff}}}. \tag{14}$$

In this equation, I_{eff} represents a weighted sum of the principal moments of inertia of the ammonia molecule. Invoking simple continuum models for solvation, Maroncelli *et al.*[46] found that the factor α_s can be expressed in terms of the molecular dipole μ, the bulk dielectric constant, and state parameters,

$$\alpha_s = \frac{4\pi\rho\mu^2}{3k_B T}\left(1 - \frac{1}{\epsilon}\right)^{-1}. \tag{15}$$

For the supercritical states of ammonia considered here, $\alpha_s^{1/2}\omega_f$ is intermediate between 25 and 40 fs^{-1},[47] values that are comparable to the fitted value for ω_s mentioned above. Although we will not claim here that the simple physical arguments that lead to Eqs. (13)–(15) should remain valid for the more complex case of the solvation of a highly quantum object in supercritical environments, it is interesting to verify that our preliminary results suggest the persistence of a certain level of correspondence between the two character-

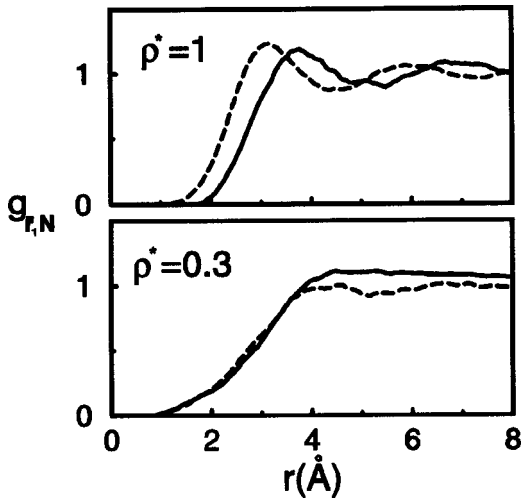

FIG. 8. Equilibrium spatial correlations between the center of the first excited state $\bar{\mathbf{r}}_1$ and the nitrogen site at two SCA densities at $T=450$ K. The solid (dashed) lines correspond to adiabatic trajectories with forces taken from the ground (first excited) state.

istic frequencies—a fact that has also been proved to hold for the case of solvation of simple anionic species in SCW.[48]

The results presented in Figs. 6 and 7 reveal faster relaxation and near absence of diffusional contributions at low density supercritical environments. In order to investigate the differences in the mechanisms through which the systems relax, we present in Fig. 8 results for the two limiting, $t=0$ and $t=\infty$, equilibrium spatial correlations between the center of the excited electronic distribution, $\bar{\mathbf{r}}_1$, and the solvent's Nitrogen site. Although, at high densities, one expects considerable rearrangements in the solvent spatial distribution around the solute due to the gross symmetry changes in the electronic wave function, the $t=0$ distribution can be practically superimposed to that corresponding to $t=\infty$, by simply operating a negative, 0.5 Å shift in the radial coordinate (upper panel). On the other hand, at low densities, the changes in the two limiting distributions are much less pronounced, and are to be found at long range. Given the observed differences in the spatial correlations, we are led to believe that the slow portions of the relaxations at high densities can be ascribed to the approaching of the solvent molecules towards the center of the electronic charge. Finally, and more importantly, notice that the shift towards smaller distances in the excited $g_{\bar{\mathbf{r}}_1\mathrm{N}}(r)$ function—a fact that in principle could be interpreted as a sign of a more confined solute—contrasts the particle-in-a-box interpretation of the reduction of the energy gap, discussed earlier in connection to the time evolution of σ_1. This indicates that the localization mechanism for excited electrons in supercritical ammonia is mainly driven by the polarization fluctuations that prevails in these environments, with only minor contributions from short ranged, excluded volume effects, arising from electron–solvent exchange forces.

IV. SUMMARY AND CONCLUDING REMARKS

We have presented path integral and plane-waves adiabatic MD simulations studies of a quantum excess electron solvated in supercritical ammonia covering a wide range of densities from diluted vaporlike ambients to the triple point density along the 450 K isotherm ($T^*=1.10$). The PIMD analysis of the equilibrium correlation length for the electron–polymer locates the transition from localized to quasifree electronic states around one fourth of the ammonia's triple point density. Overall, solvated electron size is larger in supercritical ammonia than in supercritical water at similar reduced thermodynamic states because of the stronger polarity of water. This observation agrees with experimental evidence.

Analysis of the wave function for the bound states shows a ground *s*-like state and three, quasidegenerate excited states with *p*-like characteristics. For low density ambients ($\rho^*\leqslant 0.35$) the energy gap between the two lowest lying states is comparable to the nuclear thermal energy fluctuations, suggesting that nonadiabatic effects may be relevant to the dynamical features of the electronic states. The ground state absorption spectrum computed at different solvent densities exhibits an asymmetric line shape consistent with experimental observations. However, the maximum of the computed spectrum presents considerably stronger redshifts with decreasing density than the experimental data.

The solvation dynamics subsequent to the electron photoexcitation to the first excited state has been studied within the adiabatic approximation for the time evolution of the electronic states at two reduced densities ($\rho^*=0.35$ and 1.0) and $T^*=1.10$. The solvation responses present a bimodal decay consisting of an initial fast Gaussian-type relaxation followed by a diffusive regime. At low density, the role of diffusive components seem to be marginal. These features are interpreted in the light of the dynamical history of the eigenstate energies and electron size following the sudden excitation, and the electron centroid–solvent radial distribution function.

ACKNOWLEDGMENTS

The authors gratefully acknowledge the financial support provided by the Antorchas/Vitae Foundations (Argentina/Brazil). M.S.S. also thanks CNPq and FAPESP (01/09374-3). D.L. is a member of Carrera del Investigador Científico de CONICET (Argentina).

[1] For recent advances in technological processes involving supercritical fluids, see, for example, *Innovations in Supercritical Fluids, Science, and Technology*, ACS Symposium Series 608, edited by K. W. Hutchenson and N. R. Foster (American Chemical Society, Washington, D.C., 1995).
[2] M. A. Mc Hugh and V. J. Krukonis, *Supercritical Fluid Extraction: Principles and Practice* (Butterworths, Boston, 1986).
[3] S. Kim and K. P. Johnston, in *Supercritical Fluids, Chemical, and Engineering Principles and Applications*, ACS Symposium Series 329, edited by T. G. Squires and M. E. Paulatis (American Chemical Society, Washington, D.C., 1987); S. Kim and K. P. Johnston, Ind. Eng. Chem. Res. **26**, 1206 (1987); G. E. Bennet and K. P. Johnston, J. Phys. Chem. **98**, 441 (1994).
[4] D. G. Peck, A. J. Mehta, and K. P. Johnston, J. Phys. Chem. **93**, 4297 (1989).
[5] K. P. Johnston and C. Haynes, AIChE J. **33**, 2017 (1987).
[6] V. Giraud and P. Krebs, Chem. Phys. Lett. **86**, 85 (1982).
[7] P. Krebs and M. Hientze, J. Chem. Phys. **76**, 5484 (1982).
[8] F.-Y. Jou and G. R. Freeman, J. Phys. Chem. **85**, 629 (1981).

[9] R. Olinger, U. Schinderwolf, A. Gaathon, and J. Jortner, Ber. Bunsenges. Phys. Chem. **75**, 690 (1971).
[10] R. Olinger, S. Hahne, and U. Schinderwolf, Ber. Bunsenges. Phys. Chem. **76**, 349 (1972).
[11] A. Migus, Y. Gaudel, J. L. Martin, and A. Antonetti, Phys. Rev. Lett. **58**, 1559 (1987).
[12] F. H. Long, H. Lu, X. Shi, and K. B. Eisenthal, Chem. Phys. Lett. **185**, 47 (1991).
[13] J. C. Alfano, P. K. Walhout, Y. Kimura, and P. F. Barbara, J. Chem. Phys. **98**, 5996 (1993); Y. Kimura, J. C. Alfano, P. K. Walhout, and P. F. Barbara, J. Phys. Chem. **98**, 3450 (1994).
[14] There is a large body of experimental and theoretical work devoted to electrons in supercritical noble gases. See, for example, J. A. Jahnke, L. Meyer, and S. A. Rice, Phys. Rev. A **3**, 734 (1971); S. S. S. Huang and G. R. Freeman, J. Chem. Phys. **68**, 1355 (1978); M. A. Floriano and G. R. Freeman, *ibid.* **85**, 1603 (1986); D. F. Coker, B. J. Berne, and D. Thirumalai, *ibid.* **86**, 5689 (1987); D. Laria and D. Chandler, *ibid.* **87**, 4088 (1987); B. Space, D. F. Coker, Z. H. Liu, B. J. Berne, and G. Martyna, *ibid.* **97**, 2002 (1992); B. Plenkiewicz, Y. Frongillo, J.-M. Lopez-Castillo, and J.-P. Jay-Gerin, *ibid.* **104**, 9053 (1996); J.-M. Lopez-Castillo, Y. Frongillo, B. Plenkiewicz, and J.-P. Jay-Gerin, *ibid.* **96**, 9092 (1992).
[15] P. Krebs, Chem. Phys. Lett. **70**, 465 (1980).
[16] P. Krebs, V. Giraud, and M. Wantschick, Phys. Rev. Lett. **44**, 211 (1980).
[17] M. Sprik, R. W. Impey, and M. L. Klein, J. Chem. Phys. **83**, 5802 (1985).
[18] M. Sprik and M. L. Klein, J. Chem. Phys. **87**, 5987 (1987).
[19] M. Sprik and M. L. Klein, J. Chem. Phys. **89**, 1592 (1988).
[20] M. Sprik and M. L. Klein, J. Chem. Phys. **91**, 5665 (1989).
[21] M. Marchi, M. Sprik, and M. L. Klein, J. Chem. Phys. **89**, 4918 (1988); R. N. Barnett, U. Landman, C. L. Cleveland, N. R. Kestner, and J. Jortner, Chem. Phys. Lett. **148**, 249 (1988).
[22] M. Sprik, R. W. Impey, and M. L. Klein, Phys. Rev. Lett. **56**, 2326 (1986); G. J. Martyna and M. L. Klein, J. Chem. Phys. **96**, 7662 (1992).
[23] D. Laria and M. S. Skaf, J. Phys. Chem. A **106**, 8066 (2002).
[24] A. Gaathon, G. Czapski, and J. Jortner, J. Chem. Phys. **58**, 2648 (1972); J. Jortner and A. Gaathon, Can. J. Chem. **55**, 1801 (1977).
[25] T. Bausenwein, H. Bertagnolli, A. David, K. Goller, H. Zweier, K. Todheide, and P. Chieux, J. Chem. Phys. **101**, 672 (1994).
[26] M. Kiselev, T. Kerdcharoen, S. Hannongbua, and K. Heizinger, Chem. Phys. Lett. **327**, 425 (2000).
[27] R. P. Feynmann, *Statistical Mechanics* (Addison–Wesley, Reading, 1972).
[28] R. W. Impey and M. L. Klein, Chem. Phys. Lett. **104**, 579 (1984).
[29] M. R. H. Rudge, J. Phys. B **11**, 1503 (1978); **11**, 2221 (1978); M. R. H. Rudge, *ibid.* **13**, 1269 (1980).
[30] A. Jain and D. G. Thompson, J. Phys. B **15**, L631 (1982); **16**, 1113 (1983); **16**, 2593 (1983); F. A. Gianturco, *ibid.* **24**, 4627 (1991).
[31] D. Chandler and P. G. Wolynes, J. Chem. Phys. **74**, 4078 (1981).
[32] M. E. Tuckerman, B. J. Berne, G. J. Martyna, and M. L. Klein, J. Chem. Phys. **99**, 2796 (1993); G. J. Martyna, M. E. Tuckerman, D. J. Tobias, and M. L. Klein, Mol. Phys. **87**, 1117 (1996); M. E. Tuckerman and A. Hughes, *Path Integral Molecular Dynamics: A Computational Approach to Quantum Statistical Mechanics*, in *Classical and Quantum Dynamics in Condensed Phase Simulations*, edited by B. J. Berne, G. Ciccotti, and D. F. Coker (World Scientific, Singapore, 1998), Chap. 14.
[33] J.-P. Ryckaert, G. Ciccotti, and H. J. C. Berendsen, J. Comput. Phys. **23**, 327 (1977).
[34] F. Webster, P. J. Rossky, and R. Friesner, Comput. Phys. Commun. **63**, 494 (1991).
[35] A. Staib and D. Borgis, J. Chem. Phys. **103**, 2642 (1995).
[36] C.-Y. Yang, K. F. Wong, M. S. Skaf, and P. J. Rossky, J. Chem. Phys. **114**, 3598 (2001).
[37] J. Schnitker and P. J. Rossky, J. Chem. Phys. **86**, 3471 (1987).
[38] The dielectric constant for ammonia along the supercritical $T=453$ K isotherm does not surpass, say, $\epsilon \approx 7$. For water at similar corresponding states, the values of ϵ are in most cases, at least a factor of 2 higher. See, M. Buback and W. D. Harder, Ber. Bunsenges. Phys. Chem. **81**, 603 (1977).
[39] A. Wallqvist, G. J. Martyna, and B. J. Berne, J. Phys. Chem. **92**, 1721 (1988).
[40] B. J. Schwartz and P. J. Rossky, J. Phys. Chem. **101**, 6902 (1994).
[41] B. J. Schwartz and P. J. Rossky, J. Phys. Chem. **101**, 6917 (1994). For more recent developments, see P. J. Rossky, *Nonadiabatic Quantum Dynarnics Simulation Using Classical Baths*, in *Classical and Quantum Dynamics in Condensed Phase Simulations*, edited by B. J. Berne, G. Ciccotti, and D. F. Coker (World Scientific, Singapore, 1998), Chap. 22.
[42] G. Herzberg, *Infrared and Raman Spectra of Polyatomic Molecules* (Van Nostrand, Princeton, 1945).
[43] B. J. Schwartz and P. J. Rossky, J. Phys. Chem. **105**, 6997 (1996).
[44] O. V. Prezhdo and P. J. Rossky, J. Phys. Chem. **100**, 17094 (1996).
[45] M. Maroncelli, J. Mol. Liq. **57**, 1 (1993).
[46] M. Maroncelli, P. V. Kumar, and A. Papazyan, J. Phys. Chem. **97**, 13 (1993).
[47] This value was obtained from estimates of the dielectric constant from Ref. 38 and assuming I_{eff} as the average between the different moments of inertia of the ammonia molecule.
[48] M. Re and D. Laria, J. Phys. Chem. A **101**, 10494 (1997).